

Density Functional Theory Investigation on the Structural and Electronic Properties of Pristine, Vacancy, and Group IV Doped Zigzag Boron Nitride Nanotubes

Pek-Lan Toh*, Syed Amir Abbas Shah Naqvi, Suh-Miin Wang

Faculty of Engineering and Green Technology, Universiti Tunku Abdul Rahman, 31900 Kampar, Perak, Malaysia

Abstract In this work, density functional theory (DFT) calculations were conducted to study the structural and electronic properties of pure, vacancy, and group IV [i.e. carbon (C), silicon (Si), and germanium (Ge) atoms] doped boron nitride nanotubes (BNNTs). The DFT computational results obtained agree well with the literature results. The calculated B–N bond distances obtained in this study are about 1.44 Å – 1.47 Å. Among seven BNNTs, the optimized B₃₅GeN₃₆H₁₂ holds the lowest local energy minimum value in this study. Moreover, the structure of B₃₅CN₃₆H₁₂ possesses the smallest HOMO–LUMO energy (2.17 eV) among nine BNNT models considered. The boron (B) atoms hold the positive charges, and the negative charges fall on the nitrogen (N) atoms in this work. Similar results are reported to the molecular electrostatic potentials (MEPs) of studied BNNTs. The distributions of positive and negative electrostatic potentials fall on the regions of N– and B–tips of BNNT frameworks, respectively in this report. The DFT calculations reported that the spin densities were mainly concentrated in the regions around group IV elements, such as C, Si, and Ge atoms. Therefore, we believe that these computed results will provide useful information on the adsorption of hydrogen molecules on the BNNT frameworks in the future.

Keywords: Density functional theory, boron nitride nanotube, electronic structures, HOMO-LUMO energies, molecular electrostatic potentials.

Introduction

Many experimental studies have been focused on the structure of boron nitride (BN) over the years. In 1953, Pease studied the crystal structure of boron nitride (BN), with the corresponding lattice constants of $a = b = 2.50399 \text{ \AA}$ and $c = 6.66120 \text{ \AA}$, respectively [1]. The hexagonal form of BN possesses two angles of 90° and another angle of 120° in the study. Mukasyan, in 2017 presented BN as an inorganic compound with equal numbers of N and B atoms [2]. The hexagonal boron nitride (h-BN) system is mainly used in electronic and optoelectronic devices due to its high dielectric breakdown and high resistivity. In 2020, Cahill *et al.* mentioned two crystallographic forms of BNs, i.e. cubic or hexagonal phases [3]. At the temperature of about 1560 °C – 1660 °C, the transformation of BN from cubic phase to hexagonal phase was investigated using scanning electron microscopy (SEM), transmission electron microscopy (TEM), and X-ray diffraction (XRD) analyses, respectively.

In addition, numerous theoretical investigations have also been carried out. In 2010, Tang and Cao reported the electronic structures of BN nanosheet and two hydrogenated BN frameworks, i.e. zigzag and armchair [4]. The calculations show that the hydrogenated zigzag boron nitride frameworks possess ferromagnetic metallic characteristics in the ground state. While the hydrogenated armchair BN nanostructures have wide direct band gap values, which can be used in nonmagnetic semiconductors. In addition, the computational DFT findings also noted that the electronic properties of these two zigzag

*For correspondence:
tohpl@utar.edu.my

Received: 29 May 2022

Accepted: 28 Dec. 2022

© Copyright Toh. This article is distributed under the terms of the [Creative Commons Attribution License](#), which permits unrestricted use and redistribution provided that the original author and source are credited.


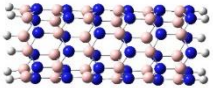

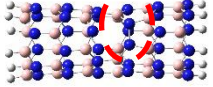

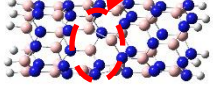

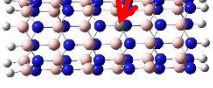

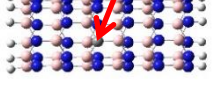

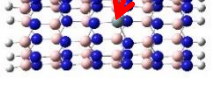
and armchair BN frameworks showed a remarkable size and structural dependence in the work. In the same year, Maryam–Mirzaei and Mahmoud–Mirzaei discussed the electronic structures of hydrogen and sulfur terminated zigzag BNNTs at the DFT/B3LYP/6–31G* level of theory [5]. The computed bond distances of B–N are about 1.44 Å– 1.48 Å in the work. These results of B–N bond lengths obtained in the work are in good agreement with those of literature studies (1.45 Å). The HOMO–LUMO energy values were determined to be 1.94 eV – 3.14 eV. Moreover, the dipole moments obtained in this work are about 6.21 debye – 8.15 debye. Among four studied frameworks (i.e. H–termination of zigzag BNNT, S_B– termination of zigzag BNNT, S_N– termination of zigzag BNNT, and S_{BN}– termination of zigzag BNNT), the S_N– termination of zigzag BNNT possesses the smallest dipole moment value. Ang *et al.*, in 2012 studied the spin density distributions of graphene cluster frameworks using Hartree–Fock (HF) and DFT methods [6]. To saturate the dangling bonds, the studied graphene cluster frameworks with the zigzag and armchair edges of graphene frameworks were terminated by hydrogen atoms in the work. Moreover, the computed findings noted the B3LYP functional is the most suitable method used to study the spin densities of pristine graphene. In 2013, Beheshtian *et al.* investigated the geometric and electronic properties of h–BN with five different organo–azo derivatives (PC–X), where PC is phenyl carbamate, X is OCH₃, CH₃, NH₂, NO₂, and CN [7]. Using B3LYP/6–31G calculations, the optimized B–N bond lengths obtained in the works are about 1.45 Å, which is in good accordance with the previous experimental and computational findings. The computed HOMO–LUMO energy values are about 4.05 eV – 5.89 eV in this report. In addition, the surface plots of Frontier molecular orbitals were also studied. The DFT results found that both HOMOs and LUMOs have shifted in the functional groups, respectively.

In the past years, many research studies have been focused on the interactions and adsorption mechanisms of BN nanostructures with other molecules due to BNs have great potential for usage in nanoscience, nanotechnology, and other applications. For example, Ponce–Pérez and Coccoletzi, in 2017 presented the hydrogenated BN nanosheets with trichloroethylene (TCE) molecules using the DFT technique [8]. There are two possible adsorption sites, such as on the top of the B atom and the top of the N atom in the report. The overall optimized bond lengths of B–N, B–H, and N–H are 1.532 Å – 1.590 Å, 1.190 Å – 1.194 Å, and 1.035 Å – 1.036 Å, respectively. In 2018, Xu *et al.* studied the geometric and electronic structures of armchair BNNTs with carmustine (CMT) and temozolomide (TMZ) using DFT calculations [9]. From the calculations, the findings noted that the closest distances of CMT/TMZ bind on the surfaces of BNNTs are determined to be 2.54 Å– 3.21 Å. Moreover, the electrostatic potential surface plots found that the outer surfaces of tubes possess negative charges, while the inner surfaces of tubes show positive charges in the work. Tang *et al.*, in 2019 studied the BN characterizations [10]. The physical and chemical results showed that the BN nanomaterials can be used as nanofillers in the future. In 2021, Chettri *et al.* reported the hydrogen storage capacity of h–BN monolayers using the DFT method [11]. The computational DFT results are similar to the literature studies. For example, the optimized bond lengths of B–N and N–N(B–B) are determined to be 1.45 Å and 2.50 Å, respectively. There are four possible molecular hydrogen adsorption sites, i.e. center, bridge, B–top, and N–top, with the corresponding binding energy of 0.175 eV – 0.212 eV per hydrogen molecule obtained in the study. Moreover, the computed hydrogen storage capacity of the BN framework is about 6.7 wt%, which is close to the value of 6.0 wt% obtained from literature surveys. Shah–Naqvi *et al.*, in 2022 presented the structural and electronic properties of BN monolayers with/without doped by group IV elements [12]. The computational findings noted that the optimized B–N bond lengths are about 1.42 Å – 1.46 Å. In the case of the molecular electrostatic potential surface maps (MEPs), the DFT findings noted that the N–edges of BN sheets show the negative electrostatic potentials, while the positive electrostatic potential surfaces fall in the regions near B–edges in the study.

Therefore, it is of great interest to carry out a computational DFT study on the local energy minima and other electronic structures of boron nitride nanotubes (BNNTs) with/without doped by group IV elements. Moreover, the details of the computational methodology, results, discussion, and conclusions are provided in the following sections.

Materials and Methods

To study the effects of surface curvature on BNNTs, the DFT technique was performed to study geometric and electronic structures of pristine, vacancy, and group IV doped BNNT frameworks. Using Gaussian 09 computational chemistry software package [13], geometry optimization calculations were carried out to find the equilibrium structures of BNNTs at the B3LYP/6–31G level of theory. Figure 1 shows the optimized geometries of BNNTs (i.e. B₃₆N₃₆H₁₂, B₃₅N₃₆H₁₂, B₃₆N₃₅H₁₂, B₃₅CN₃₆H₁₂, B₃₆N₃₅CH₁₂, B₃₅SiN₃₆H₁₂, B₃₆N₃₅SiH₁₂, B₃₅GeN₃₆H₁₂, and B₃₆N₃₅GeH₁₂). In the side views of the diagrams, both B– and N–tips were terminated with the hydrogen atoms [5, 7]. In this study, the electronic structures (i.e. total energies, Frontier molecular orbitals (FMOs), Mulliken atomic charges, and others) of BNNTs were then determined using single–point calculations at B3LYP/6–31G* level of theory.

	Top View	Side View
$B_{36}N_{36}H_{12}$		 $S = 0$
$B_{35}N_{36}H_{12}$		 $S = 1/2$
$B_{36}N_{35}H_{12}$		 $S = 1/2$
$B_{35}CN_{36}H_{12}$		 $S = 1/2$
$B_{36}N_{35}CH_{12}$		 $S = 1/2$
$B_{35}SiN_{36}H_{12}$	 Boron substituted by silicon atom	 $S = 1/2$

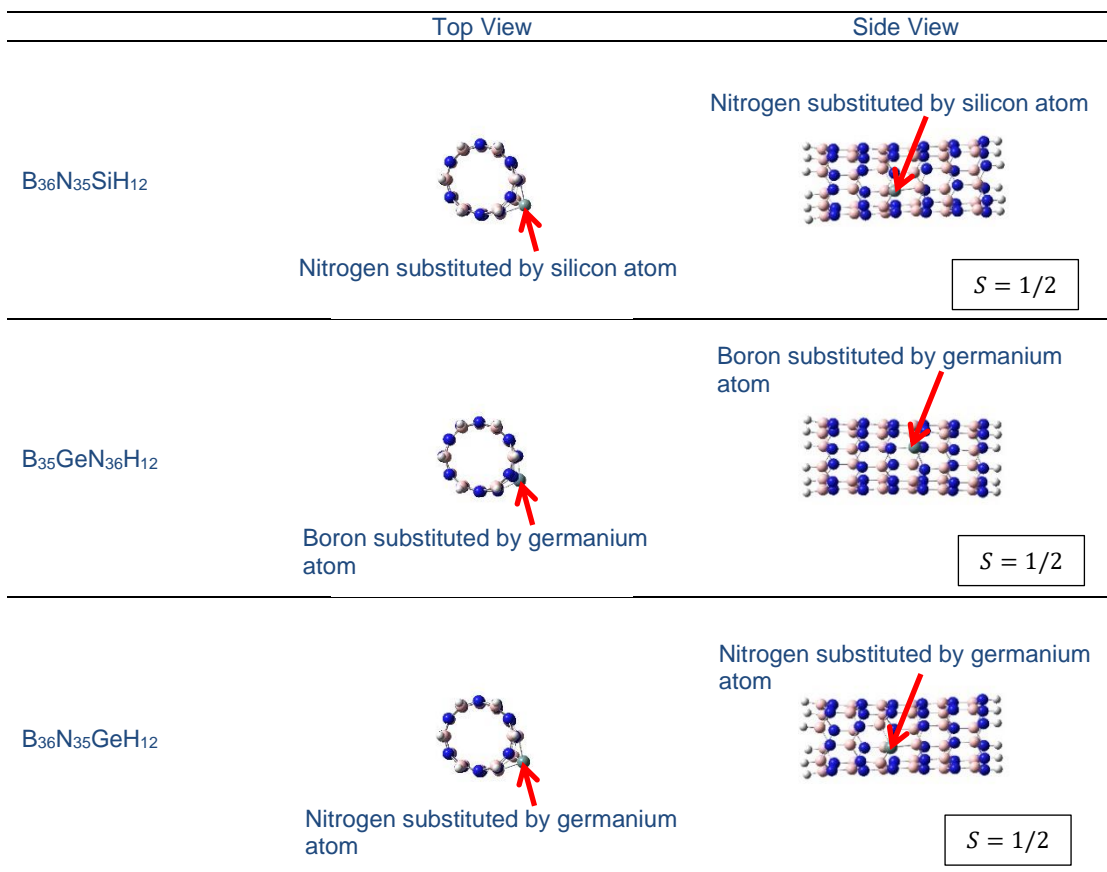


Figure 1. Optimized structures of pristine, vacancy, group IV doped BNNTs, such as $B_{36}N_{36}H_{12}$, $B_{35}N_{36}H_{12}$, $B_{36}N_{35}H_{12}$, $B_{35}CN_{36}H_{12}$, $B_{36}N_{35}CH_{12}$, $B_{35}SiN_{36}H_{12}$, $B_{36}N_{35}SiH_{12}$, $B_{35}GeN_{36}H_{12}$, and $B_{36}N_{35}GeH_{12}$

Results and Discussion

In this work, all optimized bond lengths of B–N for all studied BNNTs except $B_{36}N_{35}H_{12}$ are about 1.44 Å – 1.47 Å, which is in good agreement with the literature studies [5, 6, 11, 12]. In $B_{36}N_{35}H_{12}$, the computed B–N bond distances found around the N vacancy defect are considered to be slightly different with those of other studied BNNTs. The corresponding B–N bond lengths near N vacancy defect in $B_{36}N_{35}H_{12}$ are about 1.42 Å – 1.49 Å in this work. In Table 1, the computed total energies of pure, vacancy, and group IV doped BNNTs (i.e. $B_{36}N_{36}H_{12}$, $B_{35}N_{36}H_{12}$, $B_{36}N_{35}H_{12}$, $B_{35}CN_{36}H_{12}$, $B_{36}N_{35}CH_{12}$, $B_{35}SiN_{36}H_{12}$, $B_{36}N_{35}SiH_{12}$, $B_{35}GeN_{36}H_{12}$, and $B_{36}N_{35}GeH_{12}$) are listed. The total energy values of pristine, vacancy, and group IV BNNTs are between –134063.205 eV and –76781.621 eV in this work. Moreover, the HOMO–LUMO (highest occupied molecular orbital – lowest unoccupied molecular orbital) energies of pristine, vacancy, and group IV doped BNNTs are presented in the table. The corresponding values of HOMO–LUMO energies obtained fall in the range of 2.174 eV – 4.327 eV. These calculated HOMO–LUMO energies are close to those data reported by Maryam–Mirzaei and Mahmoud–Mirzaei [5], and slightly smaller than those of pure and group IV doped BN nanosheets presented by Shah–Naqvi *et al.* [12]. In addition, the calculated dipole moments of pure, vacancy, group IV doped BNNTs are also summarized in Table 1. The dipole moment values obtained are about 6.5364 debye – 7.0492 debye in this report. Moreover, the N-vacancy and Group IV doped on the N sites are presented to be more dipole moments if compared with B-vacancy and Group IV doped on the B sites, respectively. These dipole moments obtained from the DFT calculations are similar to the findings studied by Maryam–Mirzaei and Mahmoud–Mirzaei [5].

Table 1. Computed total energies (eV), Frontier molecular orbital energies (eV), and dipole moments (debye) of pristine, vacancy, group IV doped BNNTs

	B ₃₆ N ₃₆ H ₁₂	B ₃₅ N ₃₆ H ₁₂
Total energy	-78278.312	-77593.805
HOMO	-6.243	-5.574
LUMO	-1.916	-1.946
HOMO-LUMO	4.327	3.628
Dipole moment	6.6216	6.6827
	B ₃₆ N ₃₅ H ₁₂	B ₃₅ CN ₃₆ H ₁₂
Total energy	-76781.621	-78634.583
HOMO	-4.842	-4.047
LUMO	-1.857	-1.873
HOMO-LUMO	2.985	2.174
Dipole moment	7.0492	6.5364
	B ₃₆ N ₃₅ CH ₁₂	B ₃₅ SiN ₃₆ H ₁₂
Total energy	-77821.553	-85477.535
HOMO	-6.101	-5.830
LUMO	-1.890	-1.869
HOMO-LUMO	4.212	3.961
Dipole moment	6.8339	6.7845
	B ₃₆ N ₃₅ SiH ₁₂	B ₃₅ GeN ₃₆ H ₁₂
Total energy	-84660.591	-134063.205
HOMO	-5.937	-5.975
LUMO	-1.923	-1.852
HOMO-LUMO	4.015	4.123
Dipole moment	6.9537	6.9328
	B ₃₆ N ₃₅ GeH ₁₂	
Total energy	-133247.243	
HOMO	-5.820	
LUMO	-1.930	
HOMO-LUMO	3.890	
Dipole moment	7.0021	

Figure 2 shows the diagrams of Frontier molecular orbitals (FMOs) of pure, vacancy, and group IV doped BNNTs. The computed DFT findings in the diagrams note that the HOMO of pure BNNT is mostly constructed from the p_z -orbitals of N-tip saturated with six hydrogen atoms in the study, while the electron densities for LUMO are focused significantly on the B-tips saturated with 6 hydrogen atoms. As can be seen from the diagrams, the α -spin HOMOs of the B and N vacancy BNNTs are different with that of pristine BNNT. For both B and N vacancy BNNTs, the α -spin HOMOs are mainly located on the regions surrounding the B and N vacancy defects, respectively in this work. Moreover, the electron densities of α -spin HOMO on the case of N-vacancy are more focused in the small region surrounding N vacancy defect if compared with the B-vacancy model. Therefore, α -spin HOMO-LUMO energy of N-vacancy obtained is much smaller than that of B-vacancy. In the cases of group IV doped BNNTs, the electron density distributions of α -spin HOMOs are majority contributed from p_z -orbitals of carbon, silicon, and germanium atoms. From the α -spin HOMO diagrams, the electron density distribution of B₃₅CN₃₆H₁₂ is more concentrated than that of B₃₆N₃₅CH₁₂. Therefore, the α -spin HOMO-LUMO energy of B₃₅CN₃₆H₁₂ is calculated to be smaller than B₃₆N₃₅CH₁₂. By contrast, the distributions of electron densities for B₃₅SiN₃₆H₁₂ and B₃₆N₃₅SiH₁₂ are quite close to each other. Similarly, for B₃₅GeN₃₆H₁₂ and B₃₆N₃₅GeH₁₂, both electron density distributions are not significantly different. Therefore, the computed α -spin HOMO-LUMO of B₃₅SiN₃₆H₁₂, B₃₆N₃₅SiH₁₂, B₃₅GeN₃₆H₁₂, and B₃₆N₃₅GeH₁₂ are quite close to each other. For the α -spin LUMO of vacancy and group IV doped BNNTs, the electron density distributions are similar to that of pure BNNT framework. The electron densities of α -spin LUMOs are mainly contributed by the p_z -orbitals of B-tips for the vacancy and group IV doped BNNTs. In addition, these computed observations are close to those of pristine and group IV doped BN nanosheets reported by Shah-Naqvi *et al.* [12].

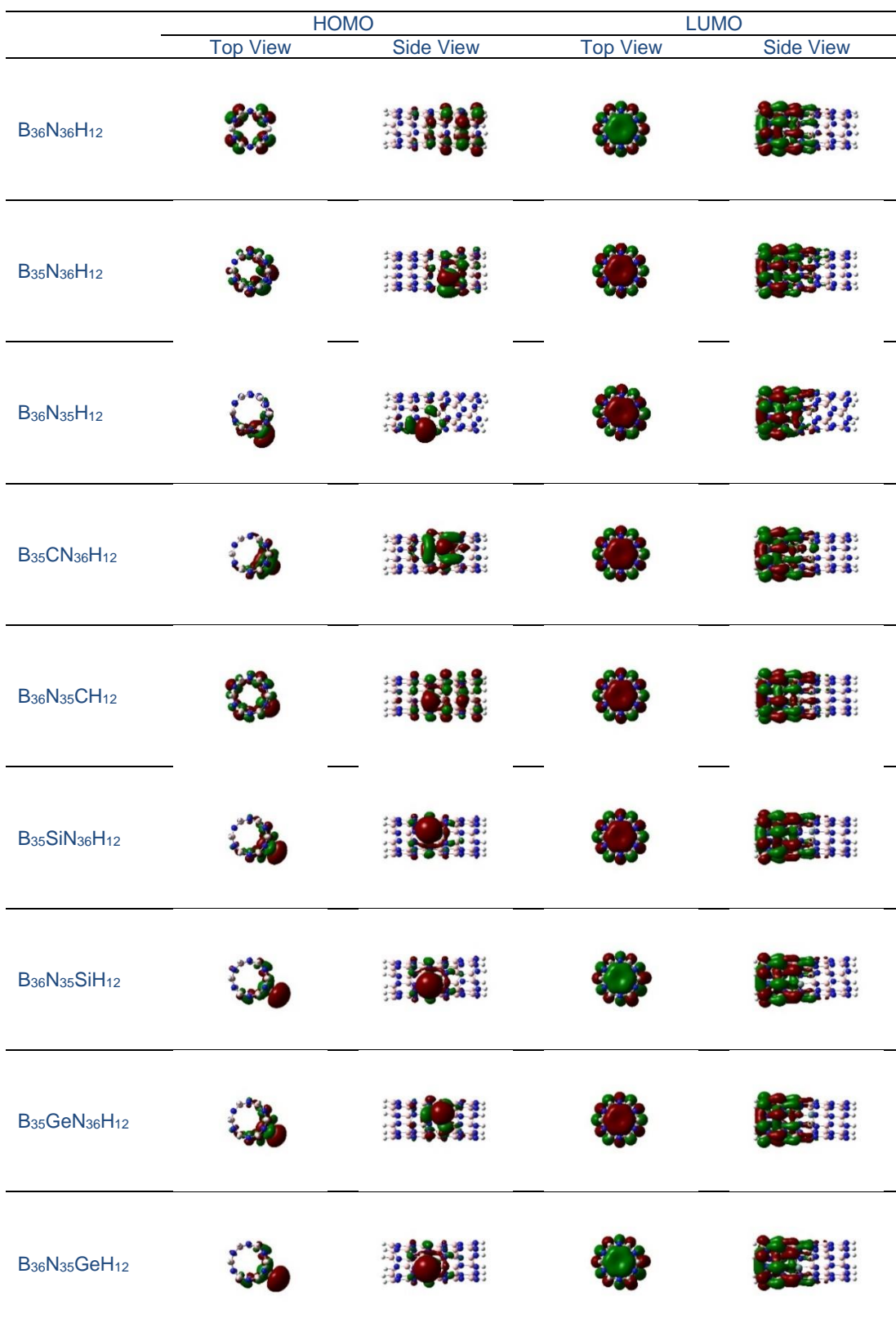
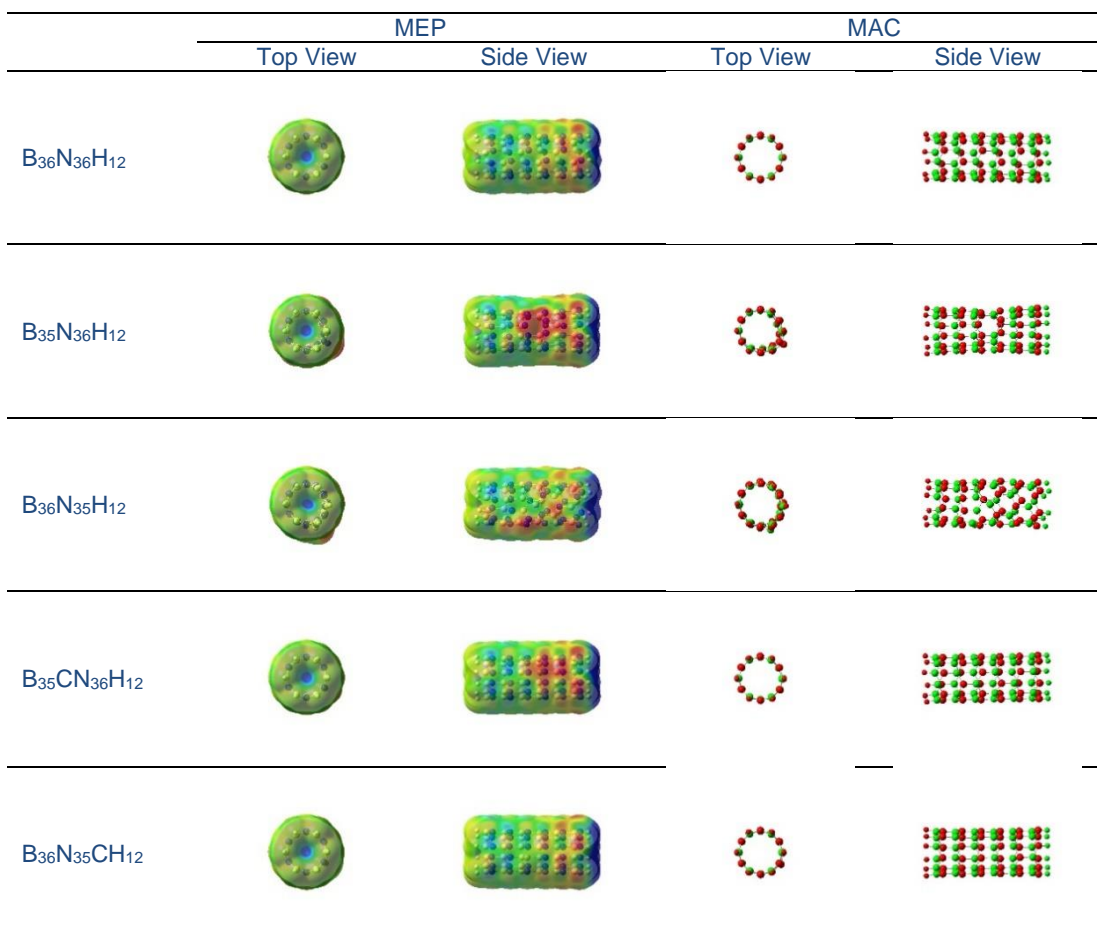


Figure 2. Frontier molecular orbital surface maps of pure, vacancy, and group IV doped BNNTs

Using a scheme of Mulliken population analysis, the computed electronic atomic charge distributions of pure, vacancy, and group IV doped BNNTs are determined. The diagrams of Mulliken atomic charge (MAC) distributions of pristine, vacancy, and group IV doped BNNTs are illustrated in Figure 3. The DFT findings note that the group IV elements (i.e. carbon, silicon, and germanium atoms) show positive and negative charges in the study. When the boron atom placed in the center of BNNT is substituted by carbon, silicon, or germanium atom, the positive charge values of group IV elements are calculated to be $0.4321 \text{ a.u.} - 0.07664 \text{ a.u.}$ in this work. While the negative charges between -0.4838 a.u. and -0.1334 a.u. are obtained from DFT calculations when the nitrogen atom located in the center of the tube is substituted by group IV elements. In this paper, all the boron atoms possess the positive charges, whereas the negative charges are found on the nitrogen atoms. In addition, the computational results also note that when boron or nitrogen atoms are placed in the center of tubes substituted by group IV element, the positive charge values of boron atoms located in N-tips are higher than those of B-tips in the studied BNNT models. While the negative charge values of nitrogen atoms located in B-tips are slightly smaller than those of N-tips. These calculated findings obtained from pristine, vacancy, and group IV doped BNNTs are close to those of pure and group IV doped BN monolayers discussed by Shah-Naqvi *et al.* [12]. Moreover, the surface maps of molecular electrostatic potentials (MEPs) of pure, vacancy, and group IV doped BNNTs are presented in Figure 3. For all studied BNNTs, the MEP map plots obtained are quite consistent to that of MAC result discussed in this study. In addition, these surface plots of MEPs are also found to be close to those of pure and group IV BN frameworks reported by Shah-Naqvi *et al.* [12]. In this report, the tips of BNNTs are saturated by twelve hydrogen atoms (i.e. B-tip is only saturated by six hydrogen atoms, and N-tip is saturated by six hydrogen atoms, respectively). From these surface plots of MEPs, the DFT results note that the regions of N-tips saturated with six hydrogen atoms show blue color surfaces in the diagrams, which means to hold the most positive electrostatic potentials contributed from the nitrogen atoms. While B-tips saturated with six hydrogen atoms possess the negative electrostatic potentials in this study.



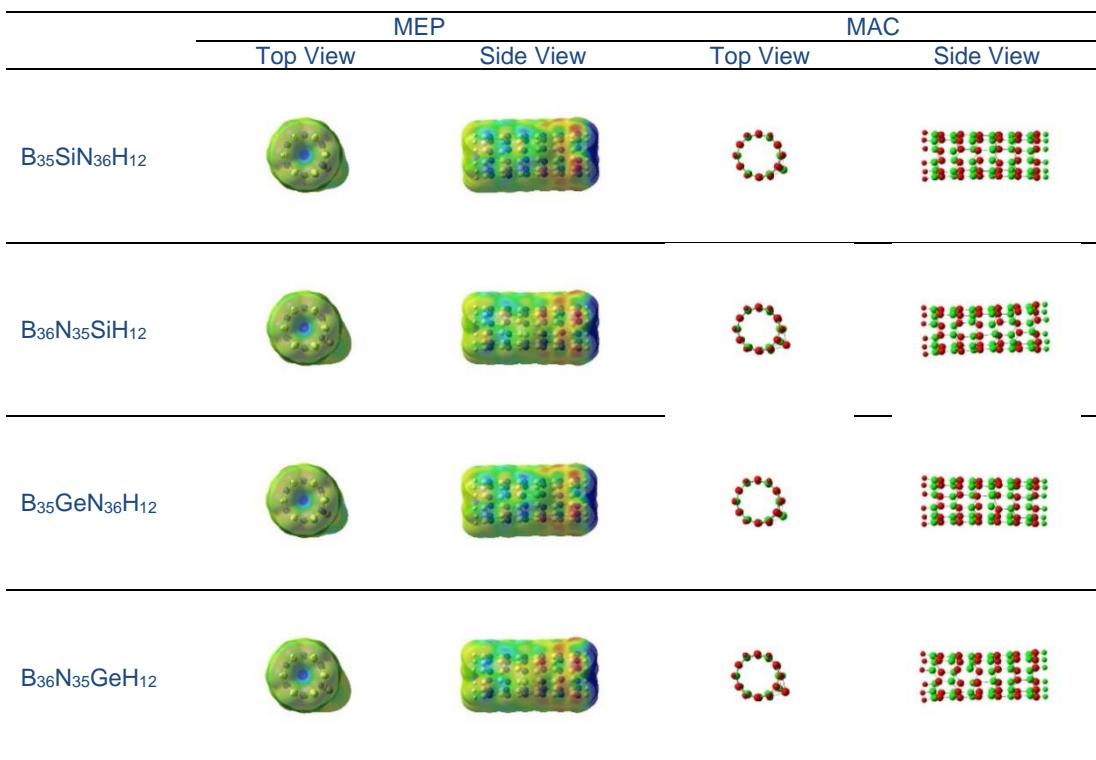
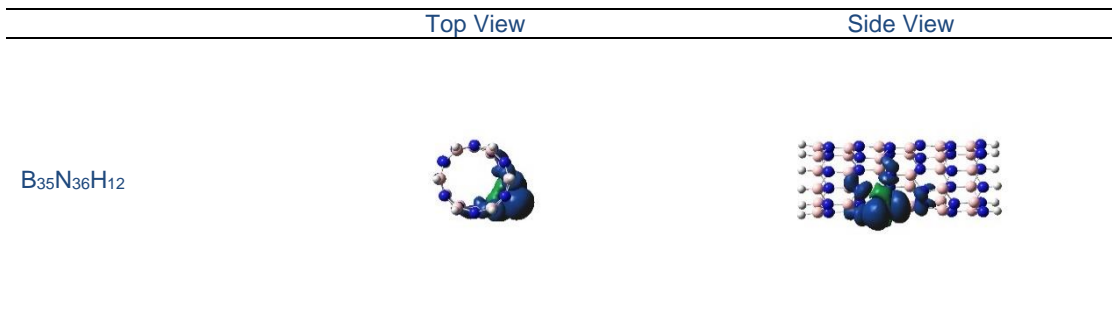

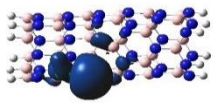

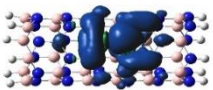

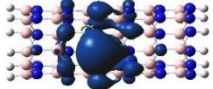
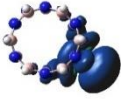
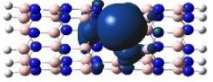
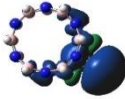
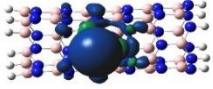
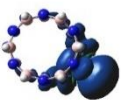
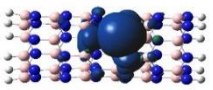


Figure 3. Molecular electrostatic potentials and Mulliken atomic charges of pure, vacancy, and group IV doped BNNTs

The spin density distributions of vacancy and group IV doped BNNTs are examined in this work. Our computed DFT findings note the spin density spin density distributions of B and N vacancy BNNTs are mainly focused on the regions surrounding the B and N vacancy defects, respectively. For example, the highest spin density distribution of B vacancy BNNT is located on the N atom, which is close to B vacancy defect in this study. The corresponding spin density of N atom is about 0.9505. While for N vacancy BNNT, the greatest spin density of B is about 0.9085. In the cases of group IV doped BNNTs, the highest spin density distributions are localized on the group IV elements, i.e. C, Si, and Ge atoms of studied BNNT frameworks. These findings are agreed well with those of BN nanosheets doped with C, Si, or Ge atom investigated by Shah–Naqvi *et al.* [12]. When one of the B atoms placed in the center of BNNTs is substituted by group IV element, the spin density values of C, Si, and Ge atoms are predicted to be 0.7113, 0.7291, and 0.6179, respectively in this study. When one of the N atoms located in the center of the nanotube is substituted by C, Si, or Ge atom, the spin densities of group IV elements are calculated to be between 0.7589 and 0.8615. These computed spin density diagrams of BNTs doped by group IV elements are presented in Figure 4. The blue color surface plots represent the positive spin densities of BNNTs doped by group IV elements, whereas the negative spin density distribution possesses the green color surface map in this work.



	Top View	Side View
$B_{36}N_{35}H_{12}$		
$B_{35}CN_{36}H_{12}$		
$B_{36}N_{35}CH_{12}$		
$B_{35}SiN_{36}H_{12}$		
$B_{36}N_{35}SiH_{12}$		
$B_{35}GeN_{36}H_{12}$		

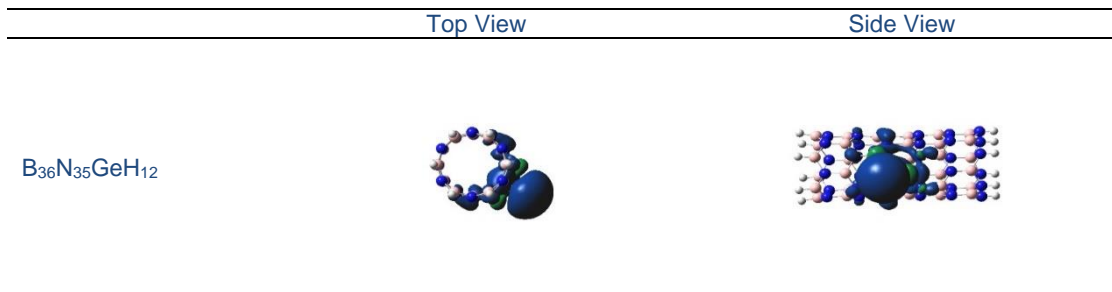


Figure 4. Computed spin density distributions of pure, vacancy, and group IV doped BNNTs

Conclusions

In this report, we apply the first-principles DFT calculations to study the total energies, FMOs, MACs, MEPs, and dipole moments of pure, vacancy, and group IV doped BNNTs. The computed results obtained are in excellent agreement with those of literature studies. For example, all optimized B–N bond distances of BNNT models are about 1.42 Å – 1.49 Å. The local energy minima of pristine, vacancy, and group IV doped BNNTs were calculated to be from –134063.205 eV to –76781.621 eV in this work. Moreover, the HOMO–LUMO energies of BNNT frameworks are about 2.174 eV – 4.327 eV. For the surface plots of FMOs, the HOMO of pristine BNNT framework has mostly p_z orbitals contributed from N–tips saturated with six hydrogen atoms. For vacancy and group IV doped BNNTs, the electron density distributions were mainly localized on the regions surrounding the vacancy defects and group IV elements of the tubes. While the LUMOs of pure, vacancy, and group IV BNNTs were composed mostly of p_z orbitals localized on the B–tips saturated with six hydrogen atoms in this study. In addition, the calculated findings also presented that all B atoms possess the positive charge values, whereas the negative charges fall on the N atoms of BNNT models. The computed charges on C, Si, Ge, and H atoms were found to be either positive or negative in this work. Similar results were investigated on the map plots of MEPs. The region near N–tips saturated with six hydrogen atoms showed the highest positive electrostatic potentials, while the negative electrostatic potentials fall on the regions near B–tips saturated with six hydrogen atoms. In the case of spin density distribution, the highest spin densities of B and N vacancy BNNTs fall on the regions surrounding the B and N vacancy defects, respectively. While the spin densities of group IV doped BNNTs were localized mostly on the group IV elements, i.e. C, Si, and Ge in this study. In general, our computational DFT results obtained noted that the studied BNNTs can be used as potential candidates for hydrogen storage nanomaterials in the future. Our further investigations are currently being carried out to study the molecular hydrogens adsorption on the outer surfaces of BNNT frameworks.

Conflicts of Interest

The author(s) declare(s) that there is no conflict of interest regarding the publication of this paper.

Acknowledgment

The research was supported by the Ministry of Higher Education (MoHE), through the Fundamental Research Grant Scheme FRGS/1/2018/TK10/UTAR/02/7.

References

- [1] Pease, R. S. (1952). An X–ray study of boron nitride. *Acta Crystallographica*, 5(3), 356-361.
- [2] Mukasyan, A. S. (2017). *Boron nitride, concise encyclopedia of self-propagating high-temperature synthesis, history, theory, technology, and products*. Netherlands: Elsevier Inc.
- [3] Cahill, J., Frane, W. D., Sio, C., King, G., Soderlind, J., Lu, R., Worsley, M., & Kuntz, J. (2020). Transformation of boron nitride from cubic to hexagonal under 1–atm helium. *Materials Science*, 109, 108078(1-8).
- [4] Tang, S. & Cao, Z. (2020). Structural and electronic properties of the fully hydrogenated boron nitride sheets and nanoribbons: insight from first-principles calculations. *Chemical Physics Letters*. 488, 67-72.
- [5] Maryam–Mirzaei & Mahmoud–Mirzaei (2010). Electronic Structure of Sulfur Terminated Zigzag Boron

- Nitride Nanotube: A Computational Study. *Solid State Science*, 12, 1337-1340.
- [6] Beheshtian, J., Soleymanabadi, H., Peyghan, A. A., & Bagheri, Z. (2013). A DFT Study on the functionalization of a BN nanosheet with PCX, (PC = Phenyl Carbamate, X= OCH₃, CH₃, NH₂, NO₂ and CN). *Applied Surface Science*, 268, 634-441.
- [7] Ang, L. S., Sulaiman, S., & Mohamed-Ibrahim, M. I. (2012). Effects of spin contamination on the stability and spin density of wavefunction of graphene: comparison between first principle and density functional methods. *Sains Malaysiana*, 41(4), 445-452.
- [8] Ponce-Pérez, R. & Coccoletzi, G. H. (2017). Hydrogenated boron nitride monolayer functionalization: a density functional theory study. *Computational and Theoretical Chemistry*, 1111, 33-39.
- [9] Xu, H, Wang, Q., Fan, G., & Chu, X. (2018). Theoretical study of boron nitride nanotubes as drug delivery vehicles of some anticancer drugs. *Theoretical Chemistry Accounts*. 137, 104(1-15).
- [10] Tang, C. Y., Zulhairun A. K., & Wong T. W. (2019). Water transport properties of boron nitride nanosheets incorporated thin film nanocomposite membrane for salt removal. *Malaysian Journal of Fundamental and Applied Sciences*, 15(6), 790-794.
- [11] Chettri, B., Patra, P. K., Hieu, N. N., & Rai, D. P. (2021). Hexagonal boron nitride (h-BN) nanosheet as a potential hydrogen adsorption material: a density functional theory (DFT) study. *Surfaces and Interfaces*. 24, 101043(1-8).
- [12] Shah-Naqvi, S. A. A., Toh, P. L., Lim, Y. C., Wang, S. M., Ang, L. S., & Sim, L. C. (2022). Computational density functional theory investigation of stability and electronic structures on boron nitride systems doped with/without group IV elements. *Malaysian Journal of Chemistry*, 24(1), 85-93.
- [13] Frisch, M. J., Trucks, G. W., Schlegel, H. B., Scuseria, G. E., Robb, M. A., Cheeseman, J. R., Scalmani, G., Barone, V., Petersson, G. A., Nakatsuji, H., Li, X., Caricato, M., Marenich, A. V., Bloino, J., Janesko, B. G., Gomperts, R., Mennucci, B., Hratchian, H. P., Ortiz, J. V., Izmaylov, A. F., Sonnenberg, J. L., Williams-Young, D., Ding, F., Lipparini, F., Egidi, F., Goings, J., Peng, B., Petrone, A., Henderson, T., Ranasinghe, D., Zakrzewski, V.G., Gao, J., Rega, N., Zheng, G., Liang, W., Hada, M., Ehara, M., Toyota, K., Fukuda, R., Hasegawa, J., Ishida, M., Nakajima, T., Honda, Y., Kitao, O., Nakai, H., Vreven, T., Throssell, K., Montgomery, J. A., Jr., Peralta, J. E., Ogliaro, F., Bearpark, M. J., Heyd, J. J., Brothers, E. N., Kudin, K. N., Staroverov, V. N., Keith, T. A., Kobayashi, R., Normand, J., Raghavachari, K., Rendell, A. P., Burant, J. C., Iyengar, S. S., Tomasi, J., Cossi, M., Millam, J. M., Klene, M., Adamo, C., Cammi, R., Ochterski, J. W., Martin, R. L., Morokuma, K., Farkas, O., Foresman, J. B., & Fox, D. J. (2016). *Gaussian 09*. United State: Gaussian, Inc.